

### **Myo Min Zaw**

Department of Mechanical Engineering,  
University of Maryland Baltimore,  
County 1000 Hilltop Circle,  
Baltimore, MD 21250  
e-mail: myo1@umbc.edu

### **William D. Hedrich**

Department of Pharmaceutical Sciences,  
University of Maryland School of Pharmacy,  
Baltimore, MD 21201  
e-mail: whedrich@umaryland.edu

### **Timothy Munuhe**

Mem. ASME  
Department of Mechanical Engineering,  
University of Maryland Baltimore,  
County 1000 Hilltop Circle,  
Baltimore, MD 21250  
e-mail: tim.munuhe@umbc.edu

### **Mohamad Hossein Banazadeh**

Department of Mechanical Engineering,  
University of Maryland Baltimore,  
County 1000 Hilltop Circle,  
Baltimore, MD 21250  
e-mail: mh.banazade@gmail.com

### **Hongbing Wang**

Department of Pharmaceutical Sciences,  
University of Maryland School of Pharmacy,  
Baltimore, MD 21201  
e-mail: hwang@rx.umaryland.edu

### **S. Andrew Gadsden**

Mem. ASME  
College of Engineering and Physical Sciences,  
University of Guelph,  
Guelph, ON N1G 2W1, Canada  
e-mail: gadsden@umbc.edu

### **Liang Zhu**

Mem. ASME  
Department of Mechanical Engineering,  
University of Maryland Baltimore,  
County 1000 Hilltop Circle,  
Baltimore, MD 21250  
e-mail: zliang@umbc.edu

### **Ronghui Ma**

Mem. ASME  
Department of Mechanical Engineering,  
University of Maryland Baltimore,  
County 1000 Hilltop Circle,  
Baltimore, MD 21250  
e-mail: roma@umbc.edu

# **Fabrication of a Cell Culture Plate With a Three-Dimensional Printed Mold and Thermal Analysis of PDMS-Based Casting Process**

*Polydimethylsiloxane (PDMS)-based casting method was used to fabricate PDMS cell culture platforms with molds printed by a fused deposition modeling (FDM) printer. Cell viability study indicated that the produced plates have the suitable biocompatibility, surface properties, and transparency for cell culture purposes. The molds printed from acrylonitrile-butadiene-styrene (ABS) were reusable after curing at 65 °C, but were damaged at 75 °C. To understand thermal damage to the mold at elevated temperatures, the temperature distribution in an ABS mold during the curing process was predicted using a model that considers conduction, convection, and radiation in the oven. The simulated temperature distribution was consistent with the observed mold deformation. As the maximum temperature difference in the mold did not change appreciably with the curing temperature, we consider that the thermal damage is due to the porous structure that increases the thermal expansion coefficient of the printed material. Our study demonstrated that FDM, an affordable and accessible three-dimensional (3D) printer, has great potential for rapid prototyping of custom-designed cell culture devices for biomedical research. [DOI: 10.1115/1.4040134]*

*Keywords: heat transfer, simulation, 3D printing, PDMS-based casting*

## **1 Introduction**

Commercially available in vitro cell culture models are widely used in drug screening to assess therapeutic efficacy and unwanted side effects [1,2]. To improve the efficiency and throughput of the screening process, it is highly desirable to formulate a cell co-culture model that enables the drug efficacy and toxicity on multiple organs to be evaluated simultaneously. Ideally, a cell

Contributed by the Heat Transfer Division of ASME for publication in the JOURNAL OF THERMAL SCIENCE AND ENGINEERING APPLICATIONS. Manuscript received October 17, 2017; final manuscript received April 4, 2018; published online July 13, 2018. Assoc. Editor: Samuel Sami.

co-culture model should allow cells derived from selected organs to share medium to include inter-organ interactions in the toxicological study [2]. Unfortunately, most commercially available cell culture plates do not accommodate user-specific medium sharing. Researchers have to design and prototype cell co-culture devices tailored to the specific research interests in their labs. Currently, polydimethylsiloxane (PDMS)-based casting is a widely adopted method in research labs to prototype biomedical fluidic devices that are designed to carry out disease diagnostics, to culture cells with a controllable microenvironment, and to examine chemical and biological processes with a high level of precision [3]. The production of such devices involves fabrication of a master mold with a negative design, curing PDMS liquid in the mold at elevated temperatures, and assembly of the device. Among these steps, fabrication of the master mold is the most time-consuming and costly process.

A number of traditional processes have been used to create master molds, which include, but are not limited to hot embossing, injection molding, laser photoablation, and photolithography [4–6]. Using a dedicated pressure equipment, hot embossing method creates a designed pattern by pressing an established mold against heated thermoplastic materials under a high pressure. Injection molding involves forcing melted thermoplastic materials into a heated mold cavity, followed by cooling down inside of the cavity. The requirement of a high-quality mold and dedicated equipment before production makes both methods time-consuming and expensive for prototyping. Laser photoablation method applies a high-powered pulsed laser to remove the material from a plate of thermoplastic material [4]. This process is inexpensive but it takes extended time to create a pattern. In addition, the mold material has to be compatible with the laser. Photolithography is a comparably complicated process involving multiple operation steps, such as mask preparing, spin coating of photoresist, baking, and UV light exposure. This method is expensive, time-consuming, and dependent on sophisticated facilities in a clean room [5]. More details about other fabrication methods and the associated advantages and disadvantages can be found in Refs. [4] and [6].

Recent development of three-dimensional (3D) printing technology has offered a simplified fabrication process to make complex structures directly from a computer aided design [7–14]. Unlike the above-mentioned conventional methods, the 3D printing technology allows for rapid prototyping of a master mold without necessitating access to expensive facilities and/or established molds. The rapid prototyping nature of this technology also offers an affordable means to enabling agile iterative design and optimization. Components of microfluidic devices and integrated functional platforms have been fabricated using various commercialized 3D printing techniques, i.e., stereolithography, digital micromirror device-based projection printing, two-photon polymerization, fused deposition modeling (FDM), inkjet, and bioprinting [7–17]. A variety of biomedical fluidic devices have been developed using 3D printing technologies [7,8,17].

Besides creation of master molds, curing of liquid PDMS polymer is another important step in soft lithography. A high curing temperature reduces the required curing time while increasing the hardness of the final product [18]. Curing temperature of the PDMS also affects the mechanical properties of the cured PDMS parts [18]. The manufacturer of the elastomer (SYLGARD 184 SILICONE ELASTOMER, Ellsworth Adhesives, WI) suggests temperature-dependent curing time, for example, 35 min at 100 °C, 20 min at 125 °C, and 10 min at 150 °C, etc [19]. These suggested curing temperatures might not be suitable for some 3D printed polymer-based molds because of their low threshold of glass transition temperature. To the authors' best knowledge, there is no existing thermal analysis of PDMS curing process.

In this study, we demonstrated a custom-designed PDMS cell co-culture plate made with an acrylonitrile-butadiene-styrene (ABS) mold. ABS was used because of its demonstrated biocompatibility and acceptable glass transition temperature for the

curing process. The master molds were generated using an FDM printer due to its affordable cost and easy access to users [7,8]. Designed with multiple inter-connected chambers, the multi-chamber cell culture plate is intended to serve as an efficient cell co-culture model that allows for user-specific medium sharing between cells housed in different compartments. The fabricated PDMS cell co-culture plates were tested for cell culture compatibility and cell viability. PDMS were cured with two different curing temperatures, and we observed that the ABS molds retained their structural integrity after curing in the oven at 65 °C for an hour, but were damaged over the same duration when the oven temperature was 10 °C higher. To understand the cause of mold damage, we also performed numerical simulation to predict and analyze the transient and steady-state temperature distribution in PDMS and the mold during the curing process.

## 2 Material and Method

The custom-designed cell co-culture plate with a diameter of 85 mm is shown in Fig. 1(a). It has a large chamber with a diameter of 27 mm located at its center and six smaller wells (18 mm in diameter) evenly distributed around the central chamber. All of the chambers are six millimeters in depth. Human primary hepatocytes are seeded in the center chamber while the cells derived from other organs including kidney, heart, and lung, are cultured in the surrounding chambers. Channels with a width of four millimeters are designed to connect a chamber with adjacent ones enabling medium sharing with the assistance of an orbital shaker. The corresponding master mold for this plate is shown in Fig. 1(b). The plate was designed using the commercial software, SOLIDWORKS.

The fabrication process involves three major steps: (1) prototyping of the mold using an FDM printer, (2) surface treatment of the mold, and (3) fabrication of PDMS platform. Each step is described in detail below.

*3D printing of the mold:* A 3D printer (TAZ 5, LULZBOT, CO) was used to print the mold using ABS filament (3 mm, LulzBot, CO). It typically took 3–4 h to print the designed mold. After molds with base thicknesses of 2 mm, 3 mm, and 4 mm were tested, we found that a minimum thickness of 3 mm is necessary to prevent the mold from warping at the chosen curing temperatures.

*Surface treatment:* The surface roughness of the printed parts with an FDM printer mainly depends on the deposited layer thickness. The FDM printer (TAZ 5, LULZBOT) allows deposition layer thickness to be adjusted in the range from 350 microns to 750 microns. Even when we used a layer thickness of 350  $\mu\text{m}$ , the printed molds still had a poor surface finishing. The uneven surface, if untreated, would be transferred to the cast PDMS part. The surface roughness of the plate would not only hinder cell

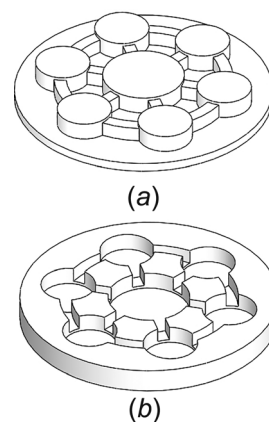


Fig. 1 (a) PDMS culture plate design and (b) mold with negative pattern

growth but also yield poor optical transparency, making it difficult to monitor cell growth under a microscope. In this study, the 3D printed mold was treated in a closed environment with several paper towels saturated with 50 ml pure Acetone (Pure Acetone Remover, MD). Usually, it took 1.5–2 h to obtain a smooth surface. The porosity of the 3D printed parts was also measured. The mold was weighted first. Then the mold was fully submerged into a beaker initially containing 300 ml of water and the total volume was read. The volume of the mold,  $V_{\text{mold}}$ , was determined as the difference between the total volume and the initial water volume. The volume of the solid ABS in the mold,  $V_{\text{abs}}$  was determined as  $m_{\text{mold}}/\rho_{\text{abs}}$ , where  $m_{\text{mold}}$  is the measured mass of the mold and  $\rho_{\text{abs}}$  is the density of the ABS material [20]. The porosity of the mold, which is defined as volumetric fraction of the pores, was calculated as  $\phi_f = 1 - V_{\text{abs}}/V_{\text{mold}}$ .

**Casting and curing of a PDMS platform:** The prepared mold was first fixed to the bottom of a Petri dish (100 mm dia.) using a double-sided adhesive. 36 g of PDMS base was homogeneously mixed with 3.6 g of the curing agent at a weight ratio of 10:1 (SYLGARD 184 SILICONE ELASTOMER, Ellsworth Adhesives, WI). Then, 39.6 g (40 ml) of the mixture was poured onto the mold fixed in the Petri dish. After degassing in a vacuum chamber (RS – 1, Best Value Vacs, Naperville, IL) for an hour, the Petri dish was placed on a piece of fire brick in an oven (10GC, Quincy Lab, Inc., Chicago, IL) preheated to a setup temperature. After curing in the oven for an hour, the PDMS part was peeled. The mold, if undamaged, could be reused. At the end of the curing process, the steady-state temperature at the top surface of cured PDMS was measured using an infrared meter (Ti100, Fluke Imager, NC) and the interior temperature on the ceiling and four sides of the oven surfaces were measured using thermal couples (copper and constantan wires, 100 micro dia. each, California Fine Wire Company, Grover Beach, CA). A thermometer at the top of the oven measured the air temperature in the oven throughout the curing process.

**Culture of human primary hepatocytes:** Human primary hepatocytes (HPH) were provided by Bioreclamation, IVT (Baltimore, MD). HPH with an initial viability greater than 90% were seeded in the PDMS plates after collagen coating at  $7.5 \times 10^5$  cells per well. Following attachment to the plates, the HPH were overlaid with matrigel (0.25 mg/mL) in serum-free Williams Medium E, forming the typical sandwich culture for hepatocyte cultures. HPH were kept in supplemented Williams Medium E and incubated at 5%  $\text{CO}_2$  and 37 °C. Cells were visualized with a Nikon Eclipse Ti Microscope.

**Cell viability assay:** HPHs were seeded at  $7.5 \times 10^5$  cells/well in collagen-coated 12-well plates or the PDMS plates following collagen coating. Cells were incubated for 72 h at 37 °C and 5%  $\text{CO}_2$ . A typical 3-[4,5-dimethylthiazol-2-yl]-2,5 diphenyl tetrazolium bromide (MTT) assay was performed. Cell viability was expressed as the percentage of the cells grown in the typical collagen-coated 12-well plates.

### 3 Numerical Modeling of Curing Process

As shown in Fig. 2, a Petri dish containing PDMS polymer and an ABS mold was placed on a piece of fire brick in the pre-heated oven for 60 min. The glass transition temperature of the ABS, which is 104 °C, sets up the upper limit of the curing temperature. Moreover, temperature difference in the mold during heating may cause warpage. To acquire information on the thermal conditions during the curing process, a heat transfer model considering conduction, convection, and radiation was developed to predict the transient and final temperature distributions in the PDMS and the ABS mold. Heat conduction in the PDMS material, the mold, and the fire brick is expressed by the traditional heat conduction equation as

$$\rho_i c_{pi} \frac{\partial T}{\partial t} = \nabla \cdot (k_i \nabla T), \quad i = 1, 2, 3 \quad (1)$$

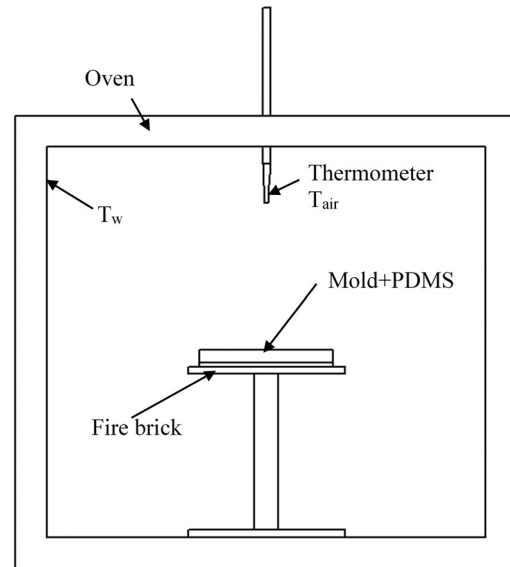


Fig. 2 Schematic of curing process in the oven

where  $\rho$  is the density,  $C_p$  is the specific heat,  $T$  is the temperature, and  $k$  is the thermal conductivity. Subscript  $i$  designates different materials, which are the PDMS, the ABS mold, and the fire brick base. Previous study shows that the volume shrinkage of PDMS after polymerization is less than 0.6% [19,21]. Therefore, the density of the PDMS is assumed constant throughout the curing process. Determining the thermal conductivity of the PDMS before complete polymerization is difficult because the rate of polymerization is unknown. Considering the temperature in the mold at the later stage of curing is more relevant to the mold deformation, we used temperature-dependent thermal conductivities of the cured PDMS in the thermal analysis of heat-induced mold deformation. The thin-walled Petri dish is not considered in the model as it has similar properties as the ABS. Perfect contact is assumed at the interfaces between the PDMS and the mold because air pockets trapped at the interface have been eliminated by the degassing process. The contact resistance between the Petri dish and firebrick is estimated to be 2.75  $\text{m}^2\text{K/W}$  based on a smooth surface of Petri dish [22] and has been included in the heat transfer model. Thermal properties of the PDMS, the ABS mold, the air, and the fire brick are given in Table 1 [19, 23–30].

For curing temperatures in the range from 60 °C to 90 °C, peak radiation in the oven falls in the infrared spectrum with a wavelength range between 8 and 8.7  $\mu\text{m}$ . The transmittance of PDMS films over this range of spectrum was studied by Chen et al. [31]. They measured the transmittance of PDMS film in the mid-infrared spectrum for three different mixing ratios of the PDMS base and curing agent: 8:1, 10:1, and 12:1. This study shows that when PDMS base and curing agent mixing ratio is 10:1, the PDMS layer has a significantly low transmittance for wavelength around 8  $\mu\text{m}$ . Therefore, we assume the 3 mm-thick PDMS layer on top of ABS as an opaque medium for radiation heat transfer.

The 3D printed products by the FDM method have porous structures and their thermal conductivities are porosity-dependent. The porosity of the 3D printed parts used in this study has been measured to be  $0.25 \pm 0.03$ . Numerous empirical models have been developed to evaluate the effective thermal conductivity of composite materials [32,33]. The Maxwell model was first introduced to evaluate effective thermal conductivity in a heterogeneous medium, but it is only validated when the porosity is less than 0.25. Many researchers modified Maxwell's model and considered different effects such as filler loading, particle size, particle shape, and homogeneity of the dispersed phase in the matrix [32,33]. For evaluating the effective thermal conductivity of 3D printed parts,

**Table 1 Thermal and physical properties of PDMS, ABS mold, air and fire brick**

Properties	PDMS	Bulk ABS	ABS mold	Air	Fire Brick
Density, $\rho$ (kg/m <sup>3</sup> )	1030 [19]	1020 [25]	764.1 <sup>a</sup>	1.177 [26]	2300 [27]
Thermal conductivity, $k$ (W/m K)	0.25 at 230 K, and 0.20 at 290 K–340 K [23]	0.17 [25]	0.122 <sup>a</sup>	0.0257 [26]	0.47 [28]
Specific heat, $C_p$ (J/kgK)	1450 [24]	1386 [29]	1038.2 <sup>a</sup>	1005 [26]	1000 [30]

<sup>a</sup>Properties of ABS mold are calculated based on porosity of 3D printed part.

**Table 2 Correlations for effective thermal conductivity**

Model	Expression	Effective thermal conductivity (W/mK)
Maxwell model [32]	$\frac{k_{\text{eff}}}{k_m} = 1 + \frac{3\phi}{\left(\frac{k_f + k_m}{k_f - k_m}\right) - \phi_f}$	0.124
Effective medium theory [32]	$\phi_m \times \frac{k_m - k_{\text{eff}}}{k_m - 2k_{\text{eff}}} + \phi_f \times \frac{k_f - k_{\text{eff}}}{k_f - 2k_{\text{eff}}} = 0$	0.121
Brueggeman [32]	$(1 - \phi_f) = \frac{(k_f - k_{\text{eff}}) \times (k_m/k_{\text{eff}})^{1/3}}{(k_f - k_m)}$	0.123
Russell [32]	$k_{\text{eff}} = k_m \times \frac{\left\{ \phi_f^{2/3} + \frac{k_m}{k_f} \cdot (1 - \phi_f^{2/3}) \right\}}{\left\{ \phi_f^{2/3} - \phi_f + \frac{k_m}{k_f} (1 + \phi_f - \phi_f^{2/3}) \right\}}$	0.122

Note:  $k_{\text{eff}}$ ,  $k_m$ , and  $k_f$  are the thermal conductivity of ABS mold, ABS polymer, and the air, respectively, and  $\phi_m$  and  $\phi_f$  are volume fraction of ABS polymer and the air, respectively.

we used the Maxwell, Effective Medium Theory, Brueggemann, and Russell methods. The expressions of the models and evaluated effective thermal conductivity are given in Table 2. The result from Russell method was used in the simulation as it emphasizes the connectivity of the solid structure, which is pertinent for 3D printed parts by an FDM printer.

The thermal conditions of the simulation are shown in Fig. 2. Before curing, the PDMS liquid and the ABS mold are at the room temperature of 20 °C. The assembly of the mold, the PDMS liquid, and the fire brick exchange heat with the surrounding environment by radiation and natural convection. As the surface area of the assembly is much smaller than the interior surface area of the oven, radiation heat transfer is approximated as radiation between a small object enclosed by a large isothermal surface. The boundary condition is thus expressed as

$$-k_i \frac{\partial T}{\partial n} = h(T - T_{\text{air}}) + \varepsilon_i \sigma (T^4 - T_w^4) \quad (2)$$

where  $T_{\text{air}}$  is the air temperature,  $T_w$  is the temperature of the interior oven surface,  $\mathbf{n}$  is the unit vector pointing outward of the part,  $\sigma$  is the Stefan-Boltzmann constant,  $\varepsilon$  is the emissivity of the PDMS or the ABS mold, and  $h$  is the heat transfer coefficient. The emissivity of the PDMS and ABS mold is 0.86 [13].  $T_{\text{air}}$  was measured by a built-in thermometer during the curing process. The air temperature was observed to be nearly constant during the curing process. According to the manufacturer of the oven, the maximum temperature variation over the interior wall surface of the oven is less than 3 °C after a steady-state is established. Our measurements confirmed that the maximum interior surface temperature variation at the curing temperatures of 65 °C and 75 °C were  $\pm 1.75$  °C and  $\pm 2.25$  °C, respectively. Thereby, the temperature variation over the interior surface of the oven was minor and therefore, neglected. Also, the air temperature measured by the thermometer at the ceiling of the oven remained nearly constant during the curing process. Therefore, the change in the surface temperature due to the placement of the PDMS was not considered either. Instead, the temperatures measured at the center of the top and the side surfaces of oven were averaged to obtain  $T_w$  to

assume a uniform oven environment. The fire brick base was preheated in the oven and was assumed to be at the same temperature as the air before curing.

The natural convection heat transfer coefficient,  $h$ , is dependent on the temperature difference between the cured parts and the surrounding environment. The heat transfer coefficient for natural convection on a horizontal surface is expressed as [22]

$$h = \frac{0.54(\text{Gr}_L \text{Pr})^{1/4} k}{L_c} \quad (3)$$

where  $\text{Gr}_L$  is the Grashof number,  $\text{Pr}$  is the Prandtl number, which is  $(\nu/\alpha)$ ,  $L_c$  is the characteristics length of the PDMS layer, and  $\nu$  and  $\alpha$  are kinematics viscosity and thermal diffusivity of the air, respectively [22]. Grashof number is defined as  $\text{Gr}_L = (g\beta(T_s - T_{\text{air}})L_c^3/\nu^2)$ , where  $g$  is the gravitational force,  $\beta$  is air thermal expansion coefficient, which is  $1/T$  for ideal gas, and  $T_s$  is the top surface temperature of the PDMS. In the numerical solution, the temperature at the center of the PDMS surface was used as  $T_s$ .

In this study, heat generation due to polymerization of PDMS is neglected after an order-of-magnitude analysis. Previous study showed that heat generation is 2.79 kJ/mol at 25 °C and 23.4 kJ/mol at 77 °C for  $D_3$  based PDMS [34]. Using the higher amount of heat generation at 77 °C, and assuming the polymerization rate is constant and is completed within 30 min, the rate of heat generation is estimated to be 0.122 W. The radiation heat transfer rate  $q_{\text{radi}}$  from the oven to the top surface of the PDMS is estimated using below equation:

$$q_{\text{radi}} = \varepsilon A \sigma (T_s^4 - T_w^4) \quad (4)$$

For a curing temperature of 65 °C, the radiation heat transfer rate is 2.8 W at the beginning of the heating and 1.2 W when the PDMS surface temperature reaches 50 °C. Since the calculated polymerization heat generation rate is one order of magnitude lower than the radiation heat transfer rate, it is neglected in this study.

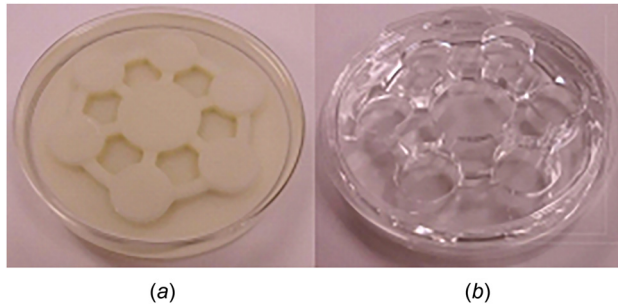


**Fig. 3** (a) A Petri dish filled with PDMS liquid after degasification and (b) a final PDMS platform after curing

The geometries of PDMS, the mold, and the fire brick base were generated and assembled in SOLIDWORKS. Then the geometry was imported into ANSYS FLUENT 18.2. A nonstructured grid system was employed to solve the heat conduction equation with the supplemented boundary conditions. A mesh with 328901 tetrahedral elements was used in the simulation. In the study of mesh dependency, a refined mesh with a doubled amount of elements yielded less than 2% difference in the maximum temperature. The second-order central scheme was used for the spatial discretization in the implicit form. A time increment of one second was used for this simulation. For each time-step, the residual of the energy equation was less than the  $10^{-6}$ . Increasing time-step to 10 s will cause a difference less than 3% in maximum temperature in the mold. Due to the limited measurement available during the curing process, the simulation was validated by comparing the measured and simulated temperature at the center of the top of the PDMS layer at the end of the curing process.

## 4 Results and Discussion

**4.1 Experimental Results.** The ABS mold after surface treatment is shown in Fig. 3(a) and the fabricated PDMS cell culture plate is displayed in Fig. 3(b). With the oven temperature set at 65 °C, the air temperature measured 60 °C and the average inner surface temperature of the oven measured 70 °C. At the end of curing, the surface temperature of PDMS was measured as 64.5 °C using an infrared thermometer. The ABS mold retained structural integrity and can be reused for curing at this temperature.

For the curing temperature of 75 °C, the air temperature measured 70 °C, and the average wall temperature of the oven was 80 °C. As shown in Fig. 4, despite its glass transition temperature of 104 °C, mold deformation occurred at the outer edge of the cylindrical column. To understand the cause of mold deformation, numerical simulation was performed to obtain the highest temperature and temperature difference in the mold during the curing process for the two curing temperatures.

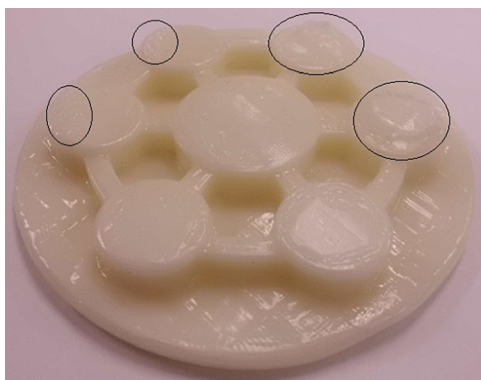


**Fig. 4** A damaged ABS mold after curing for an hour at 75 °C

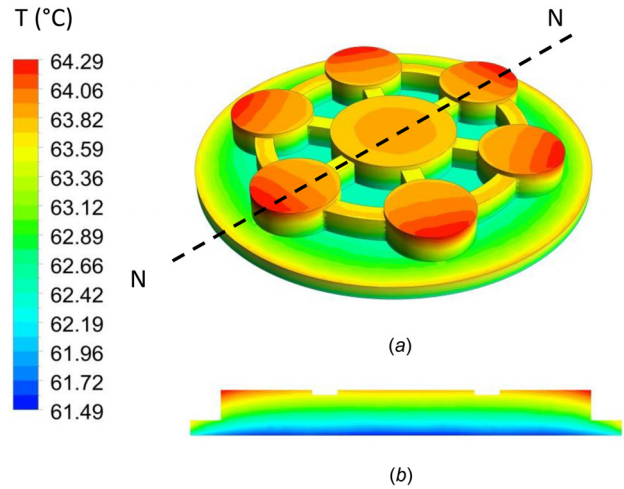


**Fig. 5** (a) Surface temperature of the ABS mold and (b) temperature distribution on the cross-sectional plane N–N after curing at 65 °C for 60 min

The temperature distributions on the ABS mold surface and on a central vertical plane after curing at 65 °C for 60 min are displayed in Figs. 5(a) and 5(b), respectively. The same results for curing at 75 °C are displayed in Figs. 6(a) and 6(b). For curing at 65 °C, the simulated temperature at the geometrical center of top PDMS surface is 63.75 °C, which is close to the measured value of 64.5 °C. We observed that the pattern of the temperature distribution is similar for these two curing temperatures. The highest temperatures and temperature gradients were observed at the outer edge of the cylindrical column. It is not surprising that deformation occurred at the same location. The largest temperature difference in the ABS mold after 60 min of curing was about 2.85 °C for curing at 65 °C and 3.23 °C for curing at 75 °C.

The simulated temperature distributions on the top PDMS surface at the end of curing are shown in Figs. 7(a) and 7(b), respectively. For both curing temperatures, the highest temperature in the mold was below the glass transition temperature of ABS, and elevated curing temperature did not significantly increase the temperature difference in the mold. If we assume that the thermal expansion coefficient of ABS is constant over the range of 65–75 °C, then temperature difference alone cannot explain the observed deformation at the edge of the cylindrical column at the higher curing temperature.

One possible explanation for this observation is the increased thermal expansion coefficient of the printed part due to the high temperature and the presence of pores in the ABS material [35–38]. Both elevated temperatures and the presence of porous structure reduce the Young's modulus of polymer-based materials decreases. The effect of porosity on the effective Young's modulus of ABS material is described by the power-law empirical relationship of Phani and Niyogi [35–38], which is expressed as

$$E = E_0 \left( 1 - \frac{p}{p_c} \right)^f \quad (5)$$

In Eq. (4),  $E_0$  is Young modulus of the bulk material,  $p_c$  is porosity of the bulk material, which is 100%,  $p$  is the porosity of the porous material, and  $f$  is a positive parameter, which depends on the grain morphology and pore geometry of porous material [36]. With a reduced Young's modulus, it is not surprising that the porous ABS structure expands more and is subject to visible deformation under a higher curing temperature. Nevertheless, quantitative characterization of the relationship between thermal expansion behavior and porosity of the printed part is needed to confirm the role of porous structure in the mold deformation.

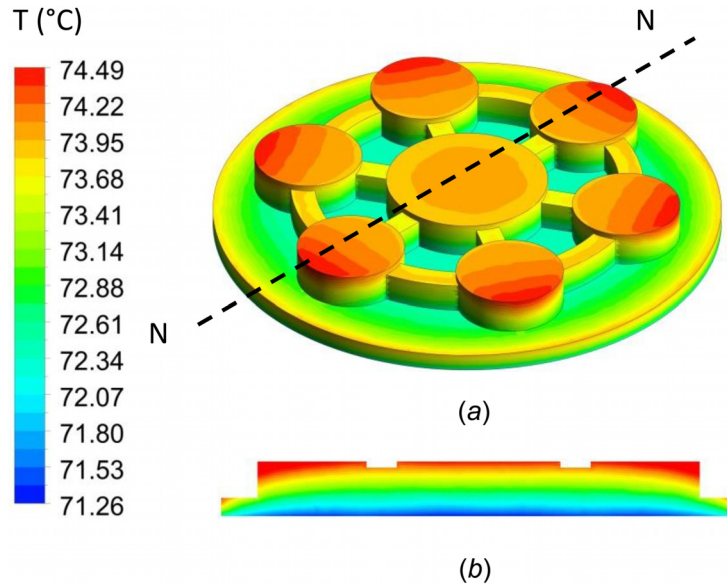


Fig. 6 (a) Surface temperature of the ABS mold and (b) temperature distribution on the cross-sectional plane N–N after curing at 75 °C for 60 min

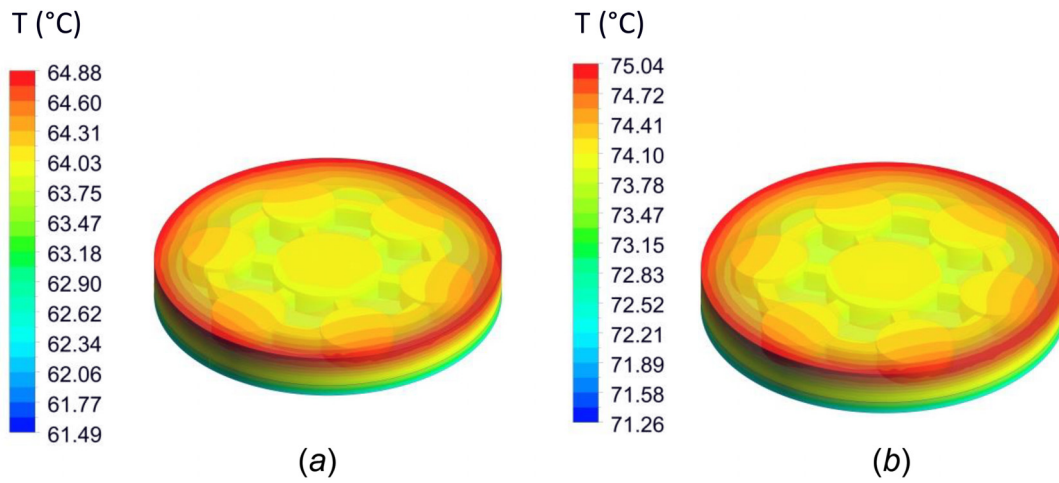


Fig. 7 Simulated surface temperature of the PDMS after curing at (a) 65 °C and (b) 75 °C for 60 min

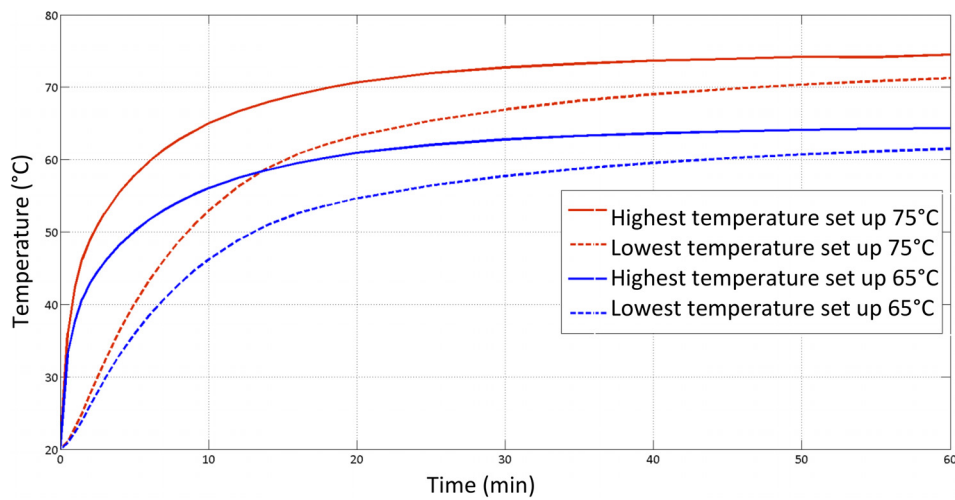


Fig. 8 The temporal evolution of the highest and the lowest temperature in the ABS mold during the curing process

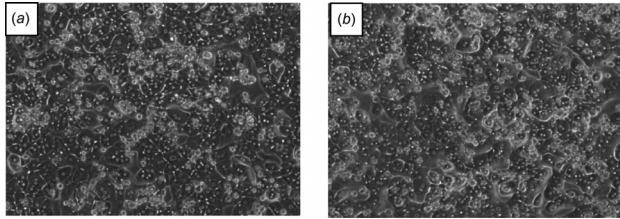


Fig. 9 (a) Cells cultured in the commercial 12 well plate and (b) in PDMS plates after 72 h

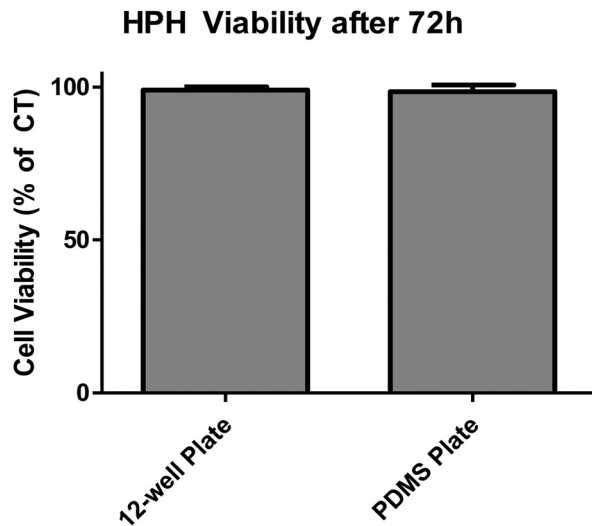


Fig. 10 Comparison of cell viability cultured in 12-well plate and PDMS plates

We also studied the transient behavior of temperature changes during the curing process. Figure 8 presents the simulated highest and lowest temperature in ABS molds throughout the curing process with different setup temperatures. The temperature in the mold increased rapidly in the first 20 min and did not change appreciably afterwards. Also, the maximum temperature difference in the first 20 min was more sensitive to curing temperature. One limitation of this study is the lack of information on the polymerization rate, which directly affects the thermal properties of the PDMS before complete polymerization. As the mold deformation occurs when the mold reaches and stays at the highest temperature during the later stage of the curing process, using the thermal properties of the cured PDMS has minor impact on the simulation of steady-state temperature distributions, but it may affect the transient behavior at the beginning the curing process.

Human primary hepatocytes cultured in the produced PDMS culture plates maintained typical morphology over a 72-h period as displayed in Fig. 9. Further, the viability of cells cultured in the PDMS plates was comparable to that of HPH cultured in standard collagen-coated 12-well plates as shown in Fig. 10. Further, a prototypical MTT assay demonstrated no difference in cell viability between HPH cultured in the two plates after 72 h. These results indicate that the PDMS plates are suitable for culture and growth of cell lines for in vitro experimentation.

## 5 Conclusion

We fabricated PDMS cell culture plates using PDMS-based casting method with 3D printed molds. Thermal analysis of the curing process was performed to understand thermal damage to the mold at elevated temperatures. The FDM, a low-cost three-dimensional printing method, was used in this study to create molds from ABS material. Cell viability studies indicate that the produced PDMS plate has the suitable biocompatibility, surface

properties, and transparency for cell culture purpose. The mold was reusable after curing at 65 °C but was damaged at temperatures far below its glass transition temperature. Numerical studies of the heating process in the mold suggest that the temperature difference is not the only cause of the observed thermal deformation at a higher curing temperature. We consider that both the high temperature and the porous structure play a role in the thermal damage. As both cause reduced Young's modulus of the structure, they increase the thermal expansion coefficient of the ABS porous structure and lead to mold deformation. With careful control of the curing process, the low-cost 3D printing technology has potential for rapid prototyping of custom-designed cell culture device for biomedical research.

## Funding Data

- This study was supported by UMB—UMBC Research and Innovation Partnership Grant, 2015–2016.

## Nomenclature

- $C_p$  = specific heat, J/(kgK)  
 $E$  = Young's modulus, Pa  
 $f$  = positive constant  
 $g$  = gravitational acceleration, m/s<sup>2</sup>  
 $Gr$  = Grashof number  
 $h$  = convection heat transfer coefficient, W/m<sup>2</sup>K  
 $k$  = thermal conductivity, W/mK  
 $k_{eff}$  = effective thermal conductivity of porous media, W/mK  
 $L_c$  = characteristic length, m  
 $m$  = mass, kg  
 $p$  = porosity of plastic porous part  
 $P_c$  = porosity of structural material of a porous part  
 $Pr$  = Prandtl number  
 $t$  = time, s  
 $T$  = temperature, K  
 $V$  = volume, m<sup>3</sup>  
 $\alpha$  = thermal diffusivity, m<sup>2</sup>/s  
 $\beta$  = thermal expansion coefficient, 1/°C  
 $\varepsilon$  = surface emissivity  
 $\nu$  = kinematic viscosity, m<sup>2</sup>/s  
 $\sigma$  = Stefan Boltzmann constant, W/K<sup>4</sup>m<sup>2</sup>  
 $\phi$  = volume fraction

## Subscripts

- abs = ABS material  
 eff = effective  
 f = fluid  
 i = material  
 m = matrix  
 w = wall

## References

- Domansky, K., Inman, W., Serdy, J., Dash, A., Lim, M. H. M., and Griffith, L. G., 2010, "Perfused Multiwell Plate for 3D Liver Tissue Engineering," *Lab Chip*, **10**(1), pp. 51–58.
- Hedrich, W. D., Xiao, J., Heyward, S., Zhang, Y., Zhang, J., Baer, M. R., Hassan, H. E., and Wang, H., 2016, "Activation of the Constitutive Androstane Receptor Increases the Therapeutic Index of CHOP in Lymphoma Treatment," *Mol. Cancer Ther.*, **15**(3), pp. 392–401.
- Halldorsson, S., Lucumi, E., Gómez-Sjöberg, R., and Fleming, R. M. T., 2015, "Advantages and Challenges of Microfluidic Cell Culture in Polydimethylsiloxane Devices," *Biosens. Bioelectron.*, **63**, pp. 218–231.
- Rodrigues, R. O., Lima, R., and Gomes, H. T., and Silva, A. M. T., 2015, "Polymer Microfluidic Devices: An Overview of Fabrication Methods," *U. Porto J. Eng.*, **1**(1), pp. 67–79.
- Friend, J., and Yeo, L., 2010, "Fabrication of Microfluidic Devices Using Polydimethylsiloxane," *Biomicrofluidics*, **4**(2), p. 026502.
- Wu, J., and Gu, M., 2011, "Microfluidic Sensing: State of the Art Fabrication and Detection Techniques," *J. Biomed. Opt.*, **16**(8), p. 080901.
- Amin, R., Knowlton, S., Hart, A., Yenilmez, B., Ghaderinezhad, F., Katebifar, S., Messina, M., Khademhosseini, A., and Tasoglu, S., 2016, "3D-Printed Microfluidic Devices," *Biofabrication*, **8**(2), p. 022001.

- [8] Ho, B., Ng, S. H., Li, H., and Yoon, Y., 2015, "3D Printed Microfluidics for Biological Applications," *Lab Chip*, **15**(18), pp. 3627–3637.
- [9] Anderson, K. B., Lockwood, S. Y., Martin, R. S., and Spence, D. M., 2013, "A 3D Printed Fluidic Device That Enables Integrated Features," *Anal. Chem.*, **85**(12), pp. 5622–5626.
- [10] Chen, C., Wang, Y., Lockwood, S. Y., and Spence, D. M., 2014, "3D-Printed Fluidic Devices Enable Quantitative Evaluation of Blood Components in Modified Storage Solutions for Use in Transfusion Medicine," *Analyst*, **139**(13), pp. 3219–3226.
- [11] Dragone, V., Sans, V., Rosnes, M. H., Kitson, P. J., and Cronin, L., 2013, "3D-Printed Devices for Continuous-Flow Organic Chemistry," *Beilstein J. Org. Chem.*, **9**, pp. 951–959.
- [12] Byun, I., Ueno, R., and Kim, B., 2014, "Micro-Heaters Embedded in PDMS Fabricated Using Dry Peel-Off Process," *Microelectron. Eng.*, **121**, pp. 1–4.
- [13] Warkiani, M. E., Khoo, B. L., Wu, L., Tay, A. K. P., Bhagat, A. A. S., Han, J., and Lim, C. T., 2016, "Ultra-Fast, Label-Free Isolation of Circulating Tumor Cells From Blood Using Spiral Microfluidics," *Nat. Protocols*, **11**(1), pp. 134–148.
- [14] Kitson, P. J., Rosnes, M. H., Sans, V., Dragone, V., and Cronin, L., 2012, "Configurable 3D-Printed Millifluidic and Microfluidic 'Lab on a Chip' Reactionware Devices," *Lab Chip*, **12**(18), pp. 3267–3271.
- [15] Bonyár, A., Sántha, H., Varga, M., Ring, B., Vitéz, A., and Harsányi, G., 2014, "Characterization of Rapid PDMS Casting Technique Utilizing Molding Forms Fabricated by 3D Rapid Prototyping Technology (RPT)," *Int. J. Mater.*, **7**(2), pp. 189–196.
- [16] Thomas, M. S., Millare, B., Clift, J. M., Bao, D., Hong, C., and Vullev, V. I., 2010, "Print-and-Peel Fabrication for Microfluidics: What's in It for Biomedical Applications?," *Ann. Biomed. Eng.*, **38**(1), pp. 21–32.
- [17] Au, A. K., Huynh, W., Horowitz, L. F., and Folch, A., 2016, "3-D Printed Microfluidics," *Angew. Chem., Int. Ed.*, **55**(12), pp. 3862–3881.
- [18] Johnston, D., McCluskey, D. K., Tan, C. K. L., and Tracey, M. C., 2014, "Mechanical Characterization of Bulk Sylgard 184 for Microfluidics and Micro-engineering," *J. Micromech. Microeng.*, **24**(3), p. 035017.
- [19] Corning, D., 2013, "Sylgard™ 184 Silicone Elastomer," Technical Data Sheet, accessed Dec. 10, 2017, <https://consumer.dow.com/content/dam/dcc/documents/en-us/productdatasheet/11/11-31/11-3184-sylgard-184-elastomer.pdf?iframe=true>
- [20] Bag, S. D., Nandan, B., Alam, S., Kandpal, L. C., and Mathur, G. N., 2003, "Density Measurements of Plastics—A Simple Standard Test Method," *Indian J. Chem. Technol.*, **10**, pp. 561–563.
- [21] Abhishek, K., 2017, "PDMS Shrinkage," University of Pennsylvania, Philadelphia, PA, accessed Dec. 10, 2017, [https://repository.upenn.edu/scn\\_protocols/42/?utm\\_source=repository.upenn.edu%2Fscn\\_protocols%2F42&utm\\_medium=PDF&utm\\_campaign=PDFCoverPages](https://repository.upenn.edu/scn_protocols/42/?utm_source=repository.upenn.edu%2Fscn_protocols%2F42&utm_medium=PDF&utm_campaign=PDFCoverPages)
- [22] Incropera, F. P., Dewitt, D. P., Bergman, T. L., and Lavine, A., 2009, *Introduction to Heat Transfer*, 5th ed., Wiley, Hoboken, NJ.
- [23] Ngo, I. L., and Byon, C., 2016, "Thermal Conductivity of Particle-Filled Polymers," *Polymer Science: Research Advances, Practical Applications, and Educational Aspects*, Formatex Research Center, Badajoz, Spain.
- [24] Livermore, C., and Voldman, J., 2004, "Design and Fabrication of Microelectromechanical Devices Material Properties Database," Massachusetts Institute of Technology, Cambridge, MA, accessed Dec. 10, 2017, <http://web.mit.edu/6.777/www/>
- [25] Styrolution, 2015, "Acrylonitrile Butadiene Styrene (ABS)," Technical Data Sheet, Styrolution, accessed Dec. 10, 2017, <http://www.activas.com.br/downloads/especialidades/abs/terluran-hh-106.pdf>
- [26] Engineering Toolbox, 2001, "Dry Air Properties Dry," The Engineering Toolbox, accessed Dec. 10, 2017, [https://www.engineeringtoolbox.com/dry-air-properties-d\\_973.html](https://www.engineeringtoolbox.com/dry-air-properties-d_973.html)
- [27] Engineering Toolbox, "Densities of Solids," The Engineering Toolbox, accessed Dec. 10, 2017, [https://www.engineeringtoolbox.com/density-solids-d\\_1265.html](https://www.engineeringtoolbox.com/density-solids-d_1265.html)
- [28] Engineering Toolbox, 2001, "Thermal Conductivity of Common Materials and Gases," The Engineering Toolbox, accessed Dec. 10, 2017, [https://www.engineeringtoolbox.com/thermal-conductivity-d\\_429.html](https://www.engineeringtoolbox.com/thermal-conductivity-d_429.html)
- [29] Granta Design, 2017, "Acrylonitrile Butadiene Styrene (ABS)," Granta Design, Cambridge, UK, accessed Dec. 10, 2017, <http://www.grantadesign.com/education/datasheets/ABS.htm>
- [30] Engineering Toolbox, 2001, "Specific Heat of Solids," The Engineering Toolbox, accessed Dec. 10, 2017, [https://www.engineeringtoolbox.com/specific-heat-solids-d\\_154.html](https://www.engineeringtoolbox.com/specific-heat-solids-d_154.html)
- [31] Chen, K.-C., Wo, A. M., and Chen, Y.-F., 2006, "Transmission Spectrum of PDMS in 4–7  $\mu\text{m}$  Mid-IR Range for Characterization of Protein Structure," *NSTI-Nanotech.*, **2**, pp. 732–735.
- [32] Iwan, S., Ando, Y., and Shimamura, S., 2006, "Theoretical Consideration of the Effect of Porosity on Thermal Conductivity of Porous Materials," *J. Porous Mater.*, **13**(3–4), pp. 439–443.
- [33] Pietrak, K., and Wiśniewski, T. S., 2015, "A Review of Models for Effective Thermal Conductivity of Composite Materials," *J. Power Technol.*, **95**(1), pp. 14–24.
- [34] Kuo, A. C. M., 1999, *Polymer Data Handbook*, Oxford University Press, New York.
- [35] Shui, Z., Zhang, R., Chen, W., and Xuan, D., 2010, "Effects of Mineral Admixtures on the Thermal Expansion Properties of Hardened Cement Paste," *Constr. Build. Mater.*, **24**(9), pp. 1761–1767.
- [36] Ghabezloo, S., 2010, "Effect of Porosity on the Thermal Expansion Coefficient: A Discussion of the Paper 'Effects of Mineral Admixtures on the Thermal Expansion Properties of Hardened Cement Paste' by Z.H. Shui, R. Zhang, W. Chen, D. Xuan," *Constr. Build. Mater.*, **24**(9), pp. 1796–1798.
- [37] Kováčik, J., 1999, "Correlation Between Young's Modulus and Porosity in Porous Materials," *J. Mater. Sci. Lett.*, **18**(13), pp. 1007–1010.
- [38] Ashby, M., 2010, "Material and Process Selection Charts," Granta Design, Cambridge, UK, accessed Dec. 10, 2017, [http://www.grantadesign.com/download/pdf/teaching\\_resource\\_books/2-Materials-Charts-2010.pdf](http://www.grantadesign.com/download/pdf/teaching_resource_books/2-Materials-Charts-2010.pdf)